Astrophys Space Sci (2011) 331: 397–408
DOI 10.1007/s10509-010-0538-0

LETTER

Redshift evolution of angular diameters and surface brightness: how rigid are galactic measuring rods?

Roman Tomaschitz

Received: 27 August 2010 / Accepted: 6 November 2010 / Published online: 18 November 2010

Abstract The effect of a cosmic time variation of Newton's constant on galactic angular diameters, linear size, apparent magnitude, and surface brightness is investigated. The redshift scaling of the gravitational constant is proportional to the Hubble parameter, derived from the constancy of a moderate dimensionless ratio of fundamental constants, and manifested in galactic linear-size evolution. The latter is demonstrated by fitting the angular size–redshift relation to spectroscopically and photometrically selected samples of high-redshift rotators. The intrinsic luminosity evolution of the rotators and their magnitude–redshift and surface brightness–redshift relations are studied. The galactic luminosity scales with a power of the Hubble parameter, and the scaling exponent is inferred from a moderate dimensionless ratio involving the gravitational constant, the Galactic luminosity, and the velocity of the Galaxy in the microwave background. The fits are performed with a cosmic expansion factor derived from paleoplanetary surface temperatures. This expansion factor is tested by comparing the corresponding redshift evolution of the angular-size distance to the distance estimates of two samples of galaxy clusters.

Keywords Time variation of the gravitational constant in Robertson–Walker cosmology · Galactic linear-size evolution · Angular diameter–redshift relation · Distance moduli and Hubble diagram of high-redshift rotators · Surface brightness–redshift relation · Galactic luminosity evolution and Tolman test

R. Tomaschitz (✉)
Department of Physics, Hiroshima University,
1-3-1 Kagami-yama, Higashi-Hiroshima 739-8526, Japan
e-mail: tom@geminga.org

1 Introduction

The purpose of this article is to provide evidence for a cosmic time variation of the gravitational constant (Dirac 1937; Teller 1948; Dyson 1972) manifested in the redshift scaling of galaxy diameters. We analyze the redshift evolution of angular and linear diameters, and argue a varying G by fitting the respective scaling functions to high-z rotators extending to redshifts up to about $z=1$ (Saintonge et al. 2008; Marinoni et al. 2008). The time variation of Newton's constant G derives from the constancy of a moderate dimensionless ratio, $\hbar^2 H_0/(G_0 c m_\pi^3)$, where m_π stands for the pion mass; subscript zeros denote present-day values. The gravitational constant linearly scales with the Hubble parameter, $G\propto H(z)$, so that the galactic linear size scales inversely with $H(z)$, which affects the angular diameter–redshift relation.

The apparent magnitude–redshift relation of the rotators and the redshift evolution of the galactic surface brightness is derived from the constancy of a second moderate dimensionless ratio, $G_0 L_0/\upsilon_0^5$, where L_0 and υ_0 denote the Galactic luminosity and velocity in the microwave background. We find a pronounced intrinsic luminosity evolution $L\propto G^9(z)$ in the distance moduli of the rotators as well as in their surface brightness, reminiscent of the solar luminosity scaling $\propto G^{15/2}$ (Gough 1981). The fits are performed with a special class of cosmic expansion factors capable of explaining the 'early faint Sun paradox' (Sagan and Chyba 1997) in the context of an open Robertson–Walker (RW) cosmology (Tomaschitz 2010).

We start with the RW line element $\mathrm{d}s^2=-c^2\,\mathrm{d}\tau^2+a^2(\tau)\,\mathrm{d}\sigma_R^2$, where $\mathrm{d}\sigma_R^2$ is the line element of a hyperbolic 3-space of curvature radius R. The expansion factor is normalized to $a(\tau_0)=1$. The ascending series of the dimensionless

scale factor $a(\tau)$ reads

$$a(\tau) = 1 + H_0(\tau - \tau_0) - \frac{q_0}{2} H_0^2 (\tau - \tau_0)^2 + \frac{p_0}{6} H_0^3 (\tau - \tau_0)^3 + \cdots. \tag{1.1}$$

Subscript zeros refer to the present epoch τ_0, e.g. $H_0 = H(\tau_0)$, where $H(\tau) = \dot{a}(\tau)/a(\tau)$. The present-day gravitational constant is $G_0 \approx 6.707 \times 10^{-45} \hbar c^5$ MeV^{-2}. The constancy of the moderate ratio

$$\frac{\hbar^2 H_0}{G_0 c m_\pi^3} \approx \frac{1}{4\pi} \tag{1.2}$$

requires the variation of the gravitational constant to be proportional to the Hubble parameter, $G \propto H(\tau)$. The pion mass, $m_\pi \approx 139.567$ MeV$/c^2$, is kept constant in the cosmic evolution, and so is Planck's constant and the speed of light. The numerical relation (1.2) is satisfied by choosing $H_0 = h_0/(9.77813\ \text{Gyr})$ with $h_0 \approx 0.6802$, so that $H_0^{-1} \approx 14.375$ Gyr. Some observational estimates of h_0 are quite close to this value (Sandage et al. 2006; Percival et al. 2010; Reid et al. 2010; Komatsu et al. 2010).

An excellent estimate of the (deceleration) parameter q_0 in (1.1) is obtained from bounds on the present-day derivative of G, such as $|\dot{G}_0/G_0| < 1.6 \times 10^{-3}$ Gyr^{-1} inferred from helioseismology (Guenther et al. 1998). The tightest bounds come from lunar laser ranging, $(4 \pm 9) \times 10^{-4}$ Gyr^{-1} (Williams et al. 2004) and $(2 \pm 7) \times 10^{-4}$ Gyr^{-1} (Müller and Biskupek 2007). These bounds suggest a q_0 very close to -1 by virtue of $\dot{G}_0/G_0 = -H_0 \varepsilon$, where $\varepsilon := 1 + q_0$. The bound of 2×10^{-4} Gyr^{-1} implies $|\varepsilon| < 2.9 \times 10^{-3}$.

In Sects. 2 and 3, we sketch the RW cosmology employed in the fits of the galactic diameters, distance moduli and surface brightness, in particular the redshift scaling of the Hubble parameter and the luminosity distance. In Sect. 4, we study angular-diameter distances of galaxy clusters, as well as the linear and angular size evolution of high-z rotators. In Sect. 5, we investigate the redshift evolution of galactic luminosities, which shows in the magnitude–redshift relation and the surface brightness of the rotators. In Sect. 6, we present our conclusions.

2 Hubble parameter as universal scaling variable

We consider a specific class of expansion factors (Tomaschitz 2010)

$$a(\tau) = A_0 \tau^\beta \sinh^\alpha(\eta\tau/\tau_0), \tag{2.1}$$

describing the crossover from an initial power law, $\propto \tau^{\alpha+\beta}$, to exponential expansion, $\propto \tau^\beta \mathrm{e}^{\alpha\eta\tau}$, in the final stage. The parameters α and η are positive, and $\gamma := \alpha + \beta \geq 0$. The latter condition is required for expansion, $\dot{a}(\tau) > 0$. The normalization $A_0 := 1/(\tau_0^\beta \sinh^\alpha \eta)$ means $a(\tau_0) = 1$. The logarithmic derivative of (2.1) reads

$$H(\tau) = \frac{\alpha\eta}{\tau_0} \coth(\eta\tau/\tau_0) + \frac{\beta}{\tau}. \tag{2.2}$$

If $\gamma > 0$, we find $H(\tau \to 0) \sim \gamma/\tau$ and $H(\tau \to \infty) \sim \alpha\eta/\tau_0$.

The parameters τ_0, q_0, and p_0 in the ascending series (1.1) are related to the expansion factor (2.1) by

$$H_0\tau_0 = \alpha\eta \coth\eta + \beta, \tag{2.3}$$

$$\varepsilon := q_0 + 1 = \frac{1}{(H_0\tau_0)^2}\left(\frac{\alpha\eta^2}{\sinh^2\eta} + \beta\right), \tag{2.4}$$

$$\delta := p_0 - 1 = \frac{2}{(H_0\tau_0)^3}\left(\alpha\eta^3 \frac{\coth\eta}{\sinh^2\eta} + \beta\right) - 3\varepsilon. \tag{2.5}$$

Paleoclimatic estimates of planetary surface temperatures were used in Tomaschitz (2005) to single out the expansion factor defined by $\alpha = 1$, $\beta = -1/2$, and $\eta = 3/2$, so that $H_0\tau_0 \approx 1.1572$, cf. (2.3). The expansion factor defined by this parameter set and used in Figs. 1–9 results in a cosmic age of $\tau_0 \approx 16.635$ Gyr and a deceleration parameter (2.4) with $\varepsilon \approx -2.786 \times 10^{-3}$; the latter determines the present-day logarithmic derivative $\dot{G}_0/G_0 \approx 1.938 \times 10^{-4}$ Gyr^{-1}. For comparison, the age of the halo giant CS 31082–001 is 15.5 ± 3.2 Gyr inferred from U/Th production ratios (Sneden et al. 2008).

We write $H(z)$ as a shortcut for $H(\tau_1(z))$, where the emission time $\tau_1(z)$ is obtained by inversion of $a(\tau_1) = 1/(1+z)$, and $a(\tau_0) = 1$ is assumed here. More explicitly, to find $\tau_1(z)$, we have to solve

$$(\eta\tau_1/\tau_0)^{\beta/\alpha} \sinh(\eta\tau_1/\tau_0) = \frac{\eta^{\beta/\alpha} \sinh\eta}{(1+z)^{1/\alpha}}. \tag{2.6}$$

We introduce the rescaled Hubble parameter $h(z) := H(\tau_1(z))/H_0$, and write the curvature radius of the hyperbolic 3-space as $R =: \hat{R}c/H_0$, so that $\hat{R}$ is the present-day curvature radius in units of c/H_0.

To obtain the low-z series of the Hubble parameter, we expand $\dot{a}(\tau_1)/a(\tau_1)$ at τ_0 by making use of (1.1), and substitute the low-z expansion of $\tau_1(z)/\tau_0$, cf. (2.6), arriving at

$$h(z) = 1 + \varepsilon z + \left(\frac{\delta}{2} + \varepsilon - \frac{\varepsilon^2}{2}\right) z^2 + \cdots, \tag{2.7}$$

where $h(z) = H(\tau_1(z))/H_0$. To derive the high-z expansion ($\tau_1(z) \to 0$) of the Hubble parameter, we substitute the as-

ymptotic inversion $\tau_1(z)/\tau_0$ of (2.6) into the ascending τ/τ_0 series of $H(\tau)$ in (2.2). Assuming $\gamma = \alpha + \beta > 0$, we obtain

$$h(z) = h_\infty (1+z)^n \left(1 + \frac{h_1}{(1+z)^{2n}} + \mathrm{O}((1+z)^{-4n})\right), \tag{2.8}$$
$$h_\infty := \frac{\gamma\eta}{H_0\tau_0}\frac{1}{(\eta^\beta \sinh^\alpha \eta)^n}, \qquad h_1 := \frac{\alpha}{2\gamma}(\eta^\beta \sinh^\alpha \eta)^{2n},$$

where $n := 1/\gamma$. By making use of the constants stated after (2.5), we find $n = 2$, $h_\infty \approx 0.2144$, and $h_1 \approx 9.136$.

3 Redshift scaling of comoving distance and luminosity distance

The comoving distance between emission at τ_1 and absorption at τ_0 reads

$$D(z) = c\int_{\tau_1}^{\tau_0} \frac{\mathrm{d}\tau}{a(\tau)} = c\tau_0 \sinh^\alpha(\eta) \int_{\tau_1(z)/\tau_0}^1 \frac{\mathrm{d}t}{t^\beta \sinh^\alpha(\eta t)}, \tag{3.1}$$

which depends on the present epoch τ_0 and on redshift by inversion of $a(\tau_1) = 1/(1+z)$, cf. (2.6). The area of a sphere of radius D in a hyperbolic 3-space of curvature $-1/R^2$ is $4\pi R^2 \sinh^2(D/R)$. The intrinsic luminosity L_b of a source relates to the apparent flux S_b by the flux–redshift relation $S_\mathrm{b} = L_\mathrm{b}/(4\pi d_\mathrm{L}^2)$, where d_L is the luminosity distance

$$d_\mathrm{L}(z) = (1+z)R\sinh\frac{D(z)}{R}. \tag{3.2}$$

We here assume frequency-integrated bolometric quantities. The Euclidean 3-space limit $R \to \infty$ is recovered by replacing $\sinh(D/R)$ by D/R. Instead of bolometric quantities, we may consider spectral densities. In the case of a power-law density, $L \propto \nu^{-s}$, we find the flux–redshift relation

$$S(\nu) = \frac{L(\nu)}{4\pi}\frac{(1+z)^{1-s}}{d_\mathrm{L}^2(z)}, \tag{3.3}$$

with flux and luminosity per unit frequency. The bolometric relation is recovered with spectral index $s = 1$.

The low-z expansion of the comoving distance $D(z)$ is based on the ascending series (1.1) of the expansion factor and subsequent term-by-term integration in (3.1). We then substitute the ascending z expansion of $\tau_1(z)/\tau_0$ as defined by (2.6) to find

$$D(z) = \frac{c}{H_0} z\left(1 - \frac{1}{2}\varepsilon z - \left(\frac{\delta}{6} + \frac{\varepsilon}{3} - \frac{\varepsilon^2}{2}\right)z^2 + \cdots\right), \tag{3.4}$$

where the numerical constants ε and δ are related to the expansion factor by (2.4) and (2.5). The low-z expansion of the luminosity distance (3.2) reads accordingly

$$d_\mathrm{L}(z) = \frac{c}{H_0} z(1+z)\left(1 - \frac{1}{2}\varepsilon z + \left(\frac{1}{6\hat{R}^2} - \frac{\delta}{6} - \frac{\varepsilon}{3} + \frac{1}{2}\varepsilon^2\right)z^2 + \cdots\right). \tag{3.5}$$

At small redshift, the dependence of the luminosity distance on the curvature radius $\hat{R}$ (in units of c/H_0, cf. after (2.6)) is apparently weak. The expansion (3.5) applies to a hyperbolic 3-space; in the case of positive spatial curvature, we replace $\hat{R}^2$ by $-\hat{R}^2$.

We turn to the high-z expansion of the metric distance $D(z)$, and restrict the parameter range to $0 < \alpha + \beta < 1$, so that the integral in (3.1) stays finite for $\tau_1 \to 0$, as suggested by planetary paleoclimates (Tomaschitz 2005). Expanding (3.1) in ascending powers of τ_1/τ_0, and substituting the high-z expansion of $\tau_1(z)/\tau_0$, we find $D(z)/R = D_\infty - D_\mathrm{h}(z)$, with the high-$z$ correction

$$D_\mathrm{h}(z) = \frac{d_\infty}{(1+z)^{n-1}}\left(1 + \frac{d_1}{(1+z)^{2n}} + \mathrm{O}((1+z)^{-4n})\right),$$
$$d_\infty := \frac{H_0\tau_0}{\hat{R}}\frac{\eta^{\beta n}\sinh^{\alpha n}\eta}{(1-\gamma)\eta}, \tag{3.6}$$
$$d_1 := -\frac{\alpha}{2\gamma}\frac{1-\gamma}{3-\gamma}\eta^{2\beta n}\sinh^{2\alpha n}\eta,$$

to the finite limit D_∞ defining the horizon,

$$D_\infty := \frac{H_0\tau_0}{\hat{R}}\sigma_\mathrm{h}\sinh^\alpha\eta, \quad \sigma_\mathrm{h} := \int_0^1 \frac{\mathrm{d}s}{s^\beta \sinh^\alpha(\eta s)}. \tag{3.7}$$

We note $\gamma := \alpha + \beta$ and $n := 1/\gamma > 1$, cf. after (2.2) and (2.8). $\hat{R}$ is the present-day curvature radius of the hyperbolic 3-space in units of c/H_0, that is, $R = \hat{R}c/H_0$, so that $c\tau_0/R = H_0\tau_0/\hat{R}$. The metric distance of the horizon is RD_∞, and the subtracted correction $RD_\mathrm{h}(z)$ accounts for finite z. The high-z asymptotics of the luminosity distance $d_\mathrm{L}(z)$ in (3.2) is found by substituting expansion (3.6) into $\sinh(D_\infty - D_\mathrm{h})$.

Remark The formalism developed here also applies to conformally coupled tachyons in an RW cosmology (Tomaschitz 2000b, 2000c). We just have to replace the speed of light by the superluminal velocity υ_t. For instance, the metric distance at absorption time τ_0 is $D(z)\upsilon_\mathrm{t}/c$ if the spacelike connection is established by superluminal quanta of speed υ_t emitted at τ_1, cf. (3.1). The tachyon mass conformally scales as $m_\mathrm{t} = m_{\mathrm{t},0}/a(\tau)$. This conformal scaling renders tachyonic wave propagation dispersion free in vacuum, and υ_t stays constant in the cosmic evolution. The tachyonic horizon is $RD_\infty(c \to \upsilon_\mathrm{t})$, so that tachyons with speed υ_t received at the present epoch were emitted within a hyperbolic

sphere of this radius; the radius of the tachyonic horizon increases by a factor of $\upsilon_t/c > 1$ as compared to the photonic counterpart. The energy of the superluminal quanta conformally scales as $E = E_0/a(\tau)$, and so does their frequency, $\nu = \nu_0/a(\tau)$. Energy and velocity are related by the tachyonic Lorentz factor $\gamma_t = (\upsilon_t^2/c^2 - 1)^{-1/2}$ via $E_0 = m_{t,0}c^2\gamma_t$. In brief, the photonic horizon can be arbitrarily extended by sufficiently speedy low-energy tachyons.

We summarize the input parameters used for the angular-size distance in Fig. 1 and the fits to the rotator samples in Figs. 2–9. The expansion factor (2.1) is specified by

$$\begin{aligned} &\alpha = 1, \qquad \beta = -1/2, \qquad \eta = 3/2, \\ &\gamma = \alpha + \beta = 1/2, \qquad n = 1/\gamma = 2. \end{aligned} \tag{3.8}$$

Based on these parameters, we derive $H_0\tau_0 \approx 1.157$ and $\tau_0 \approx 11.315/h_0$ Gyr, cf. (2.3), and note $c/H_0 \approx 2.998 \times 10^3/h_0$ Mpc with $h_0 \approx 0.680$, cf. after (1.2), and 1 Gyr $\approx 3.1557 \times 10^{16}$ s. The parameters defining the low-z expansions are $\varepsilon \approx -2.786 \times 10^{-3}$ and $\delta \approx 0.4245$, see (2.4) and (2.5). The numerical constants in (3.6) are $d_\infty \approx 4.664/\hat{R}$ and $d_1 \approx -1.827$, and the horizon in (3.7) is defined by $D_\infty \approx 3.070/\hat{R}$ and $\sigma_h \approx 1.2459$. The fits of the angular diameters in Figs. 2 and 3 and of the magnitude–redshift relation in Figs. 6 and 7 are performed in the Euclidean regime with $\hat{R} = 10$, cf. after (2.6). That is, these fits are not affected by curvature radii exceeding the Hubble distance c/H_0 by a factor of ten; the same holds for the angular-diameter distance plotted in Fig. 1.

4 Manifestation of a varying gravitational constant in the linear and angular size evolution of high-z rotators

The time scaling of galaxy diameters $y(\tau)$, i.e. their linear size evolution, is the same as of planetary orbital radii (Tomaschitz 2005), inversely proportional to the gravitational constant, which in turn scales linearly with the Hubble parameter, so that $y(\tau) \propto 1/H(\tau)$ or

$$y(z) = \frac{y_d}{h(z)}. \tag{4.1}$$

Here, y_d is the present-day diameter, and $h(z)$ the rescaled redshift-parametrized Hubble parameter $H(\tau_1(z))/H_0$. $y(z)$ is the linear size of the source at emission time $\tau_1(z)$, see (2.6). The ascending z series of the linear diameter reads, cf. (2.7),

$$y(z) = y_d\left(1 - \varepsilon z - \left(\frac{\delta}{2} + \varepsilon - \frac{3}{2}\varepsilon^2\right)z^2 + \cdots\right). \tag{4.2}$$

On substituting the constants listed after (3.8), we obtain

$$y(z) = y_d\left(1 + 2.79 \times 10^{-3} z - 0.209 z^2 + \cdots\right). \tag{4.3}$$

By making use of the asymptotic Hubble parameter (2.8), we find the high-z expansion of the linear diameter,

$$y(z) = \frac{y_d}{h_\infty}\frac{1}{(1+z)^n}\left(1 - \frac{h_1}{(1+z)^{2n}} + \cdots\right). \tag{4.4}$$

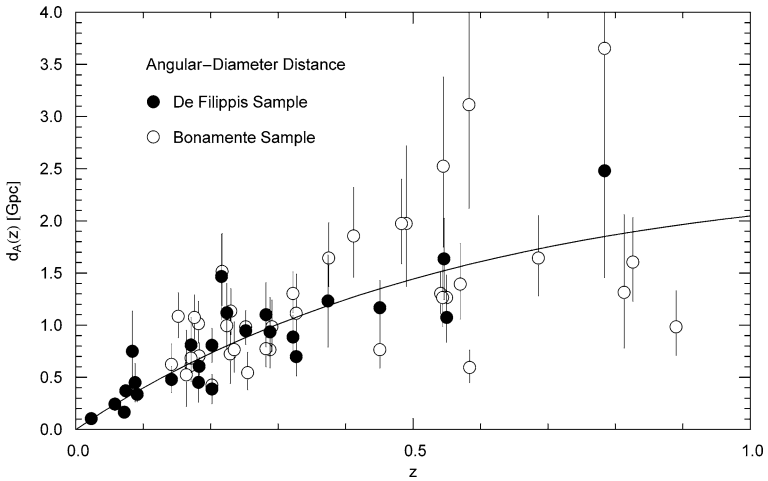

Fig. 1 Angular-size distance of two samples of galaxy clusters. Data points from De Filippis et al. (2005) and Bonamente et al. (2006). The distance estimates were obtained from measurements of the Sunyaev–Zeldovich effect (with the interferometric OVRO and BIMA arrays) and from X-ray surface brightness observations (mainly by ROSAT and Chandra). The Bonamente sample consists of 38 galaxy clusters; a spherical isothermal β model (without central X-ray cuts) is used for the intracluster medium. The De Filippis sample comprises 25 clusters compiled from Reese et al. (2002) and Mason et al. (2001), and is based on an elliptical and mostly isothermal β model. The *solid curve* shows the angular-size distance $d_A(z)$ defined in (4.5) and (3.2). Instead of (3.2), we may equally well employ the low-z expansion (3.5) of the luminosity distance in the indicated redshift range $z \leq 1$, which is virtually indistinguishable from the exact expression (3.2) used in the plot and calculated via (2.6) and (3.1). The input parameters regarding space expansion and curvature are summarized in (3.8) and thereafter

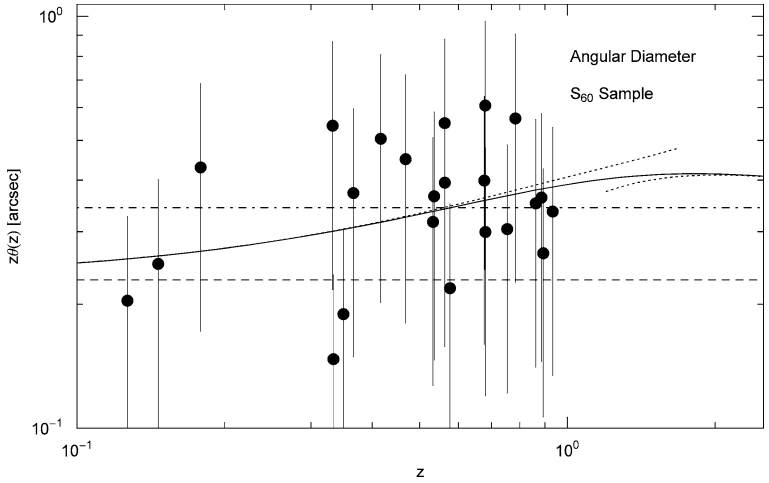

Fig. 2 Angular-size evolution of the S_{60} rotators. This sample comprises 23 galaxies with mean rotational velocity of 60.1 km/s. Data points from the VVDS and GOODS surveys (Marinoni et al. 2008). The angular diameter $\theta(z)$ is normalized with z, so that the *dashed horizontal line* stands for the Euclidean diameter $\theta_E \propto 1/z$. The fit is performed with $\theta(z)$ in (4.5) (*solid curve*) and the expansion factor specified in (3.8). The dotted curves depict the ascending z-series (4.7) of $\theta(z)$ and the high-z asymptotics (4.8). The rescaled angular diameter $z\theta(z)$ has a maximum in the crossover regime at $z \approx 1.81$, and then it monotonically decays approaching a finite limit; the low- and high-z asymptotes of $z\theta(z)$ are indicated by the *dashed* and *dot-dashed horizontal lines*. The S_{60} sample is fitted with a standard rod of size $y_d \approx 4.9$ kpc

At high z, the linear size scales as $y \propto (1+z)^{-n}$, with exponent $n = 1/\gamma$, cf. (3.8). The scaling exponents of the linear-size evolution inferred from radio galaxies and quasars typically range in an interval $1 \le n \le 3$ (Oort et al. 1987; Barthel and Miley 1988; Singal 1988, 1993; Kapahi 1989; Neeser et al. 1995; Blundell et al. 1999; Lacy et al. 1999). The scaling exponents depend on the expansion factor used in the luminosity distance when converting angular sizes into linear diameters; they also depend on the curvature radius, a Euclidean 3-space is usually assumed.

Angular diameters scale as

$$\theta(z) = \frac{y(z)}{d_A(z)}, \quad d_A(z) := \frac{d_L(z)}{(1+z)^2}. \tag{4.5}$$

The angular-size distance $d_A(z)$ is just the luminosity distance d_L in (3.2) rescaled with a redshift factor, so that $d_A(z)$ is the metric distance at emission time. Converted into arcseconds, $\theta = 2.063 \times 10^5\, y(z)/d_A(z)$. The low-$z$ expansion of the angular diameter is assembled from $d_L(z)$ in (3.5) and $y(z)$ in (4.2),

$$\theta(z)[\text{rad}] = y_d \frac{H_0}{c}\frac{1+z}{z}\left(1 - \frac{\varepsilon}{2}z - \left(\frac{1}{6\hat{R}^2} + \frac{\delta}{3} + \frac{2}{3}\varepsilon - \frac{3}{4}\varepsilon^2\right)z^2 + \cdots\right). \tag{4.6}$$

On substituting the constants stated after (3.8), we find

$$\theta(z)[\text{arcsec}] = y_d[\text{kpc}]\frac{h_0}{14.53}\frac{1+z}{z}\left(1 + 1.39 \times 10^{-3} z - \left(\frac{1}{6\hat{R}^2} + 0.140\right)z^2 + \cdots\right). \tag{4.7}$$

The Euclidean scaling $\theta_E \propto 1/z$ is recovered in the limit $z \to 0$.

The high-z asymptotics of the angular diameter is obtained from the luminosity distance $d_L(z)$ in (3.2) and expansion (4.4) of the linear diameter:

$$\theta(z) = \frac{y_d}{\hat{R}h_\infty}\frac{H_0}{c}\frac{(1+z)^{1-n}}{\sinh(D_\infty - D_h(z))} \times \left(1 - \frac{h_1}{(1+z)^{2n}} + \cdots\right), \tag{4.8}$$

where we substitute the high-z expansion of the metric distance into the hyperbolic sine; the asymptotic series $D_h(z)$ is stated in (3.6) and the constant D_∞ in (3.7).

In Fig. 1, we plot the angular-size distance $d_A(z)$ in (4.5) versus two samples of galaxy clusters specified in De Filippis et al. (2005) and Bonamente et al. (2006). The cluster distances are obtained from interferometric imaging of the Sunyaev–Zeldovich effect with arrays of the Owens Valley Radio Observatory (OVRO) and the Berkely–Illinois–Maryland observatory (BIMA), combined with ROSAT and Chandra X-ray spectroscopy (Mason et al. 2001; Reese et al. 2002; Bonamente et al. 2006). An isothermal β model is used for the intracluster plasma in both samples; spherical symmetry is assumed in the Bonamente sample, whereas the distance estimates of the De Filippis sample are corrected for ellipsoidal cluster shape (oblate spheroids). The consistency of these two data sets with the luminosity distances of a recent sample of Type Ia supernovae is discussed in Holanda et al. (2010). The angular-diameter distance in Fig. 1 is based on the luminosity dis-

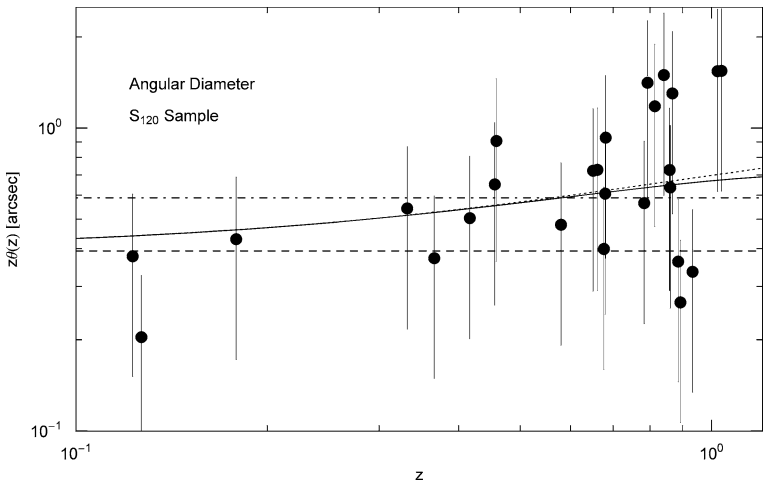

Fig. 3 Angular size–redshift relation of the S_{120} rotators. Notation as in Fig. 2. The S_{120} sample comprises 26 galaxies with average rotational speed of 120.7 km/s. The size of the standard rod used as fitting parameter is $y_d \approx 8.4$ kpc, cf. (4.1) and (4.5). The low-z asymptotics (4.7) is depicted by the *dotted curve*. The *dashed* and *dot-dashed horizontal lines* indicate the low- and high-z limits of $z\theta(z)$, which reaches a maximum at $z \approx 1.81$ as in Fig. 2

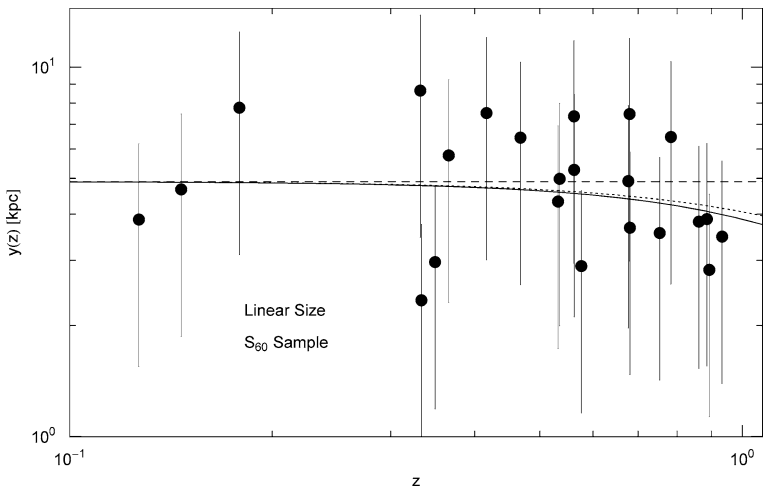

Fig. 4 Linear-size scaling of the S_{60} rotators. Data points as in Fig. 2, converted to linear diameters with the luminosity distance (3.2) and the expansion factor defined in (2.1) and (3.8). The *solid curve* depicts the linear diameter $y(z)$ in (4.1), with Hubble parameter (2.2) and redshift parametrization obtained by inversion of (2.6). The *dotted curve* shows the ascending low-z expansion (4.3) of the linear size. The *dashed horizontal asymptote* is the size of the standard rod, $y_d \approx 4.9$ kpc, extracted from the angular-diameter fit in Fig. 2

tance $d_L(z)$ defined in (3.1) and (3.2), with the emission time $\tau_1(z)$ in the metric distance (3.1) obtained by numerical inversion of (2.6). The expansion factor is specified in (3.8), a Euclidean 3-space geometry is assumed. We may also use the low-z expansion (3.5) of $d_L(z)$ in the plotted redshift range, with a curvature radius $\hat{R} \geq 10$. The angular-diameter distance $d_A(z)$ is completely specified by the expansion factor and the curvature radius, so that there is no free fitting parameter left in the plot shown in Fig. 1.

The angular-diameter fits of the rotator samples in Figs. 2 and 3 give standard rods of linear size $y_d \approx 4.9$ kpc and 8.4 kpc, respectively. y_d is the only fitting parameter; all other parameters regarding the RW cosmology are input and listed after (3.8). The data points in the figures are from Marinoni et al. (2008), compiled from the VIMOS-VLT Deep Survey (VVDS) and the Great Observatories Origins Deep Redshift Survey (GOODS). The sample S_{60} plotted in Fig. 2 comprises 23 galaxies with rotational speed between 26 and 100 km/s, with an average speed of 60.1 km/s. In Fig. 3, the rotator sample S_{120} comprises 26 galaxies with rotational speed between 60 and 204 km/s, with average speed of 120.7 km/s. This overlapping partition of the data set into an S_{60} and S_{120} sample is suggested by the nearly linear size–rotation velocity relation (Saintonge et al. 2008) manifested in the two standard rods and the corresponding mean rotational velocities. The fits in Figs. 2 and 3 can be compared to the angular diameters of various samples of radio galaxies in Nilsson et al. (1993), Dabrowski et al. (1995), Buchalter et al. (1998), and Gurvits et al. (1999).

In Figs. 4 and 5, we show the linear size evolution of the rotator samples, using the same standard rods y_d as in Figs. 2 and 3. The data points are obtained by a rescaling of the half-light angular diameters tabulated in Marinoni et al. (2008) with the angular-size distance $2d_A(z)$, cf. (4.5); for the latter, we use the luminosity distance (3.2) in the Euclidean regime with $\hat{R} = 10$, see after (3.8). One may compare these fits to the linear size evolution of the radio galaxy and quasar samples mentioned after (4.4).

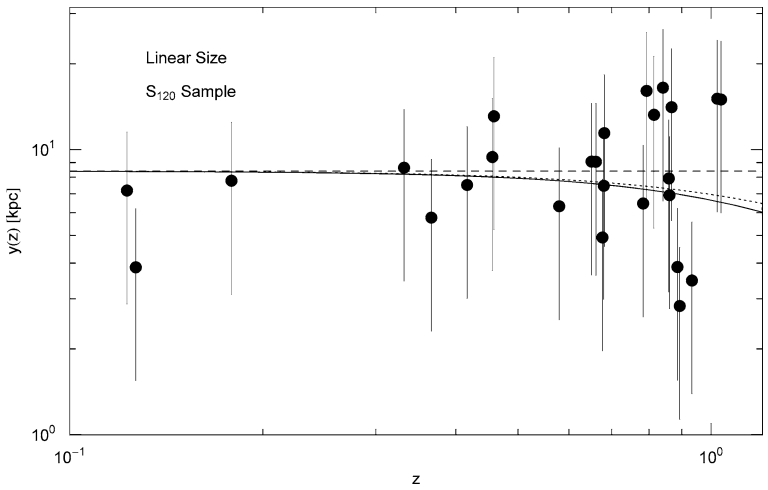

Fig. 5 Linear-size evolution of the S_{120} rotators. Data points as in Fig. 3, converted to linear diameters. Notation as in Fig. 4. The *solid curve* shows the linear diameter $y(z)$ in (4.1), with standard rod $y_d \approx 8.4$ kpc (*dashed asymptote*) extracted from the least-squares fit in Fig. 3. The low-z asymptotics (4.3) of the linear diameter is depicted as *dotted curve*

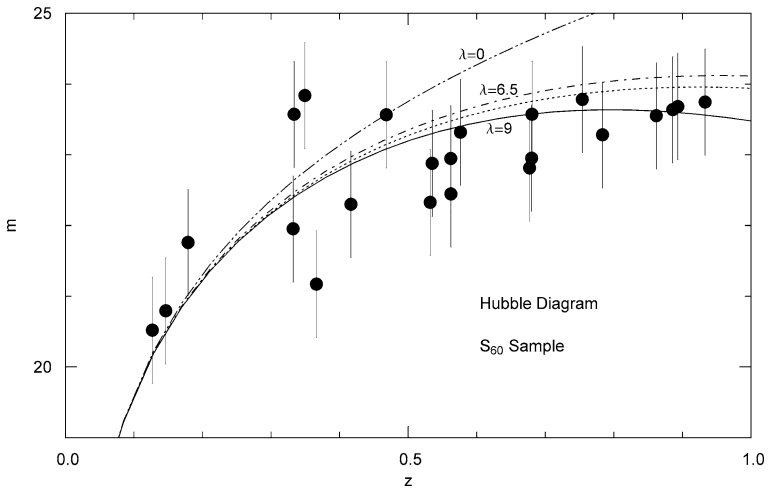

Fig. 6 Hubble diagram of the S_{60} rotators, cf. caption to Fig. 2. Data points from Marinoni et al. (2008). The fit (*solid curve*) depicts the apparent magnitude $m(z)$ in (5.2), with luminosity scaling exponent $\lambda = 9$ and space expansion (3.8). $m_{\lambda=9}(z)$ attains a maximum at $z \approx 0.80$. The absolute magnitude $M \approx -18.8$ in (5.2) is the only fitting parameter. The *dotted curve* shows the ascending low-z expansion of $m_{\lambda=9}(z)$. For comparison, we also indicate $m_{\lambda=6.5}(z)$ at the same M (*dot-dashed curve*), cf. after (5.1); the *double-dot-dashed curve* depicts $m_{\lambda=0}(z)$ in the absence of luminosity evolution

5 Luminosity evolution affecting the magnitude–redshift relation and the Tolman surface brightness test

To relate the galactic luminosity evolution $L \propto H^{\lambda}(z)$ to a moderate dimensionless ratio, we start with $G_0/c^5 \approx 2.756 \times 10^{-60}$ s/erg and note $\upsilon_{G,0}/c \approx 1/478$ as well as $L_{G,0} \approx 2 \times 10^{10} L_{\odot}$ or 7.7×10^{43} erg/s, where $\upsilon_{G,0}$ is the velocity of the Galaxy in the microwave background and $L_{G,0}$ its luminosity (Nakamura et al. 2010; Sandage et al. 2010). We thus find the moderate ratio

$$\frac{G_0 L_{G,0}}{\upsilon_{G,0}^5} \approx \frac{1}{190}. \tag{5.1}$$

On substituting $L_G = L_{G,0} h^{\lambda}(z)$, $\upsilon_G = \upsilon_{G,0} h^{\vartheta}(z)$, and $G = G_0 h(z)$ into the ratio $G L_G / \upsilon_G^5$, we find $\lambda = 5\vartheta - 1$ as condition on the exponents for this ratio to stay constant. $h(z)$ is the rescaled Hubble parameter, cf. after (2.6). It is therefore not surprising that scaling exponents related to galactic luminosity are rather large, cf. the luminosity scaling of the AGN space density in Tomaschitz (2010) ($\lambda = 6$) and the solar luminosity scaling in Gough (1981) ($\lambda = 7.5$). In contrast, the best fit of the SN Ia Hubble diagram in Tomaschitz (2010) was obtained with a mild luminosity evolution ($\lambda = 1$) corresponding to a metallicity correction to SN Ia magnitudes suggested in Gallagher et al. (2008). In Figs. 6–9, we illustrate galactic luminosity evolution with velocity scaling exponents ϑ of 1/5, 3/2, and 2, the actual fits being done with $\vartheta = 2$, that is $\lambda = 9$.

In the bolometric flux–redshift relation, cf. after (3.1), the luminosity evolution $L_b \propto h^{\lambda}(z)$ implies the flux scaling

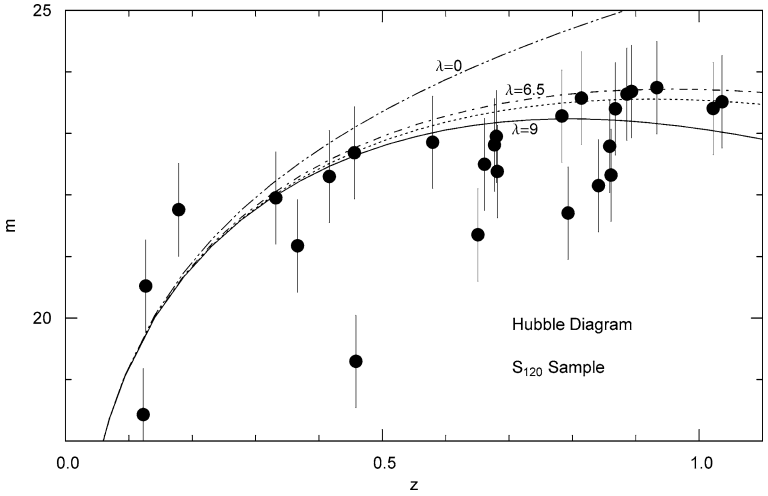

Fig. 7 Apparent magnitude–redshift relation of the S_{120} rotators, cf. Fig. 3. Notation as in Fig. 6. The *solid curve* shows the fit of the apparent magnitude $m_{\lambda=9}(z)$ in (5.2) with $M \approx -19.2$. The *dotted curve* indicates the low-z expansion of $m_{\lambda=9}(z)$, cf. after (5.2). The *dot-dashed* and *double-dot-dashed curves* depict $m(z)$ at the same absolute magnitude, with luminosity scaling exponent $\lambda = 6.5$ and $\lambda = 0$, respectively

$S(z) \propto h^{\lambda}(z)/d_{\mathrm{L}}^2(z)$, so that the magnitude–redshift relation reads

$$m(z) = 5\log\bigl(h^{-\lambda/2}(z) d_{\mathrm{L}}(z)[\mathrm{Mpc}]\bigr) + M + 25. \tag{5.2}$$

In the Hubble diagrams in Figs. 6 and 7, we fit the S_{60} and S_{120} rotator samples, see after (4.8). The fits are performed with the apparent magnitude (5.2), employing the luminosity distance $d_{\mathrm{L}}(z)$ in (3.2), the comoving distance (3.1), and the emission time obtained by numerical inversion of (2.6). The parameters (3.8) (determining the expansion factor) and the luminosity scaling exponent $\lambda = 9$ are input, and the absolute magnitude serves as fitting parameter; we find $M \approx -18.8$ for the S_{60} rotators in Fig. 6, and $M \approx -19.2$ for the S_{120} sample in Fig. 7. In the figures, we also show the low-z asymptotics of $m(z)$, calculated with the ascending z series of the Hubble parameter in (2.7) and $d_{\mathrm{L}}(z)$ in (3.5), without further expanding the logarithm in (5.2). In the redshift range up to $z \approx 1$, the fits are not sensitive to curvature radii above $\hat{R} = 10$, see after (3.8).

The redshift scaling of the surface brightness, $\mathrm{SB} = S/\theta^2$, is derived from the flux–redshift relation (3.3) and the angular size–redshift relation (4.5),

$$\mathrm{SB}(z) = \frac{L}{4\pi y_{\mathrm{d}}^2} \frac{h^{2+\lambda}(z)}{(1+z)^{3+s}}. \tag{5.3}$$

The spectral index $s = 1$ gives the bolometric brightness which, in the absence of size and luminosity evolution, results in the Tolman scaling $\mathrm{SB} \propto (1+z)^{-4}$ (Lubin and Sandage 2001; Sandage 2010). By contrast, $\mathrm{SB}(z)$ in (5.3) is based on the linear size evolution $\propto 1/h(z)$, cf. (4.1), and the luminosity scaling $\propto h^{\lambda}(z)$, cf. after (5.1). The low-z expansion of (5.3) reads

$$\mathrm{SB}(z) = \frac{L}{4\pi y_{\mathrm{d}}^2} \frac{1}{(1+z)^{3+s}} \times \left(1 + \varepsilon z + \left(\frac{\delta}{2} + \varepsilon - \frac{1}{2}\varepsilon^2\right) z^2 + \cdots\right)^{2+\lambda}, \tag{5.4}$$

where we have used $h(z)$ in (2.7) and $\theta(z)$[rad] in (4.6). The high-z asymptotics is obtained from (2.8):

$$\mathrm{SB}(z) = \frac{L}{4\pi y_{\mathrm{d}}^2} h_{\infty}^{2+\lambda} (1+z)^{(2+\lambda)n-3-s} \times \bigl(1 + h_1 (1+z)^{-2n} + \cdots\bigr)^{2+\lambda}. \tag{5.5}$$

It is not efficient to further expand (5.4) and (5.5) because of the large exponents, see below. The ellipses in (4.4), (4.8), and (5.5) stand for terms of $\mathrm{O}((1+z)^{-4n})$.

The fits of the S_{60} and S_{120} rotator samples in Figs. 8 and 9 are performed with

$$\mathrm{SB}(z)[\mathrm{Jy/arcsec^2}] = 1.87 \times 10^{-12} \frac{L[\mathrm{Jy\,kpc^2}]}{y_{\mathrm{d}}^2[\mathrm{kpc}]} \frac{h^{2+\lambda}(z)}{(1+z)^{3+s}}. \tag{5.6}$$

The standard rods $y_{\mathrm{d}} \approx 4.9$ kpc and 8.4 kpc are taken from the angular-diameter fits in Figs. 2 and 3, respectively. We specify the space expansion as in (3.8), and use the bolometric photon index $s = 1$ and the luminosity scaling exponent $\lambda = 9$ as in the Hubble diagrams in Figs. 6 and 7. The data points in Figs. 8 and 9 are obtained by converting the AB magnitudes in Marinoni et al. (2008) to flux densities via $m + 48.6 = -(5/2)\log(S/10^{23}\mathrm{Jy})$, and by a subsequent rescaling of the flux densities with the inverse squared angular diameters (4.7). We note $1\,\mathrm{Jy\,kpc^2} \approx 9.52 \times 10^{19}\ \mathrm{erg\,s^{-1}\,Hz^{-1}}$. The luminosity per unit frequency is used as fitting parameter; we find $L \approx 1.62 \times$

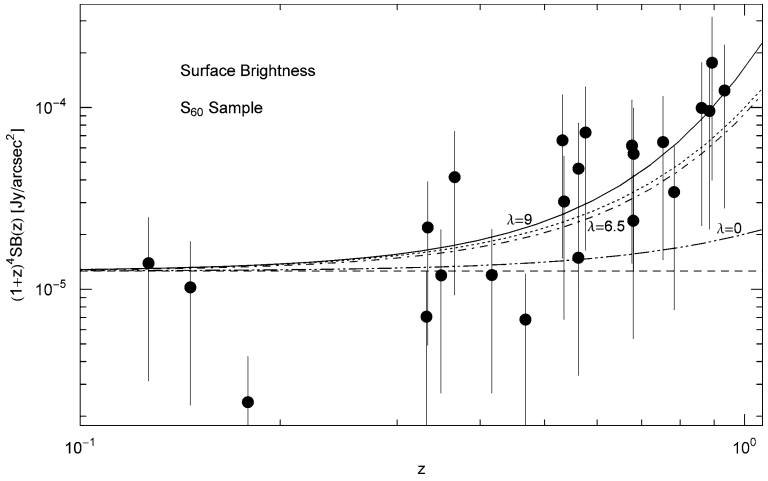

Fig. 8 Surface brightness of the S_{60} rotator sample, cf. Figs. 2, 4, and 6. Data points from the VVDS and GOODS surveys, obtained by conversion of the AB magnitudes tabulated in Marinoni et al. (2008), cf. after (5.6). The χ^2 fit (*solid curve*) is based on the surface brightness $\mathrm{SB}(z)$ in (5.6), normalized to the Tolman prediction $\mathrm{SB} \propto (1+z)^{-4}$. The latter assumes absence of intrinsic size and luminosity evolution, cf. (4.1) and after (5.1), and is indicated by the *dashed horizontal line*. The fit is performed with the luminosity scaling exponent $\lambda = 9$, the bolometric photon index $s = 1$, and a standard rod of size $y_\mathrm{d} \approx 4.9$ kpc as inferred from the angular-size fit in Fig. 2 with the same expansion factor (3.8). The luminosity of the standard rod is the only fitting parameter, $L \approx 1.62 \times 10^8$ Jy kpc^2, cf. (5.6). The low-z asymptotics of $\mathrm{SB}(z)$ in (5.4) is depicted as *dotted line*. The *dot-dashed curve* is a plot of $\mathrm{SB}(z)$ with the same parameters apart from the luminosity exponent $\lambda = 6.5$. The *double-dot-dashed curve* shows the surface brightness without luminosity evolution, $\lambda = 0$

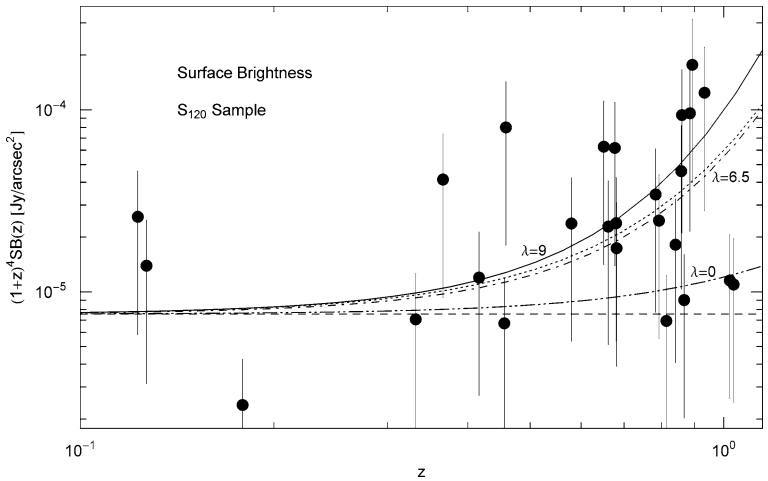

Fig. 9 Surface brightness–redshift relation of the S_{120} rotators, cf. Figs. 3, 5, and 7. Notation as in Fig. 8. The *solid curve* depicts $\mathrm{SB}(z)$ in (5.6), with input parameters $\lambda = 9$, $s = 1$, and $y_\mathrm{d} \approx 8.4$ kpc, the latter obtained from the angular diameters in Fig. 3. The luminosity per unit frequency of the standard rod y_d is extracted from the least-squares fit, $L \approx 2.85 \times 10^8$ Jy kpc^2. The Tolman scaling is indicated by the *dashed horizontal line*, and the low-z expansion (5.4) of $\mathrm{SB}(z)$ by the *dotted curve*. The *dot-dashed* and *double-dot-dashed curves* show $\mathrm{SB}(z)$ with luminosity scaling exponent $\lambda = 6.5$ and $\lambda = 0$, respectively, cf. after (5.1)

10^8 Jy kpc^2 for the S_{60} rotators in Fig. 8, and $L \approx 2.85 \times 10^8$ Jy kpc^2 for the S_{120} sample in Fig. 9. The fits in Figs. 8 and 9 clearly differ from the Tolman prediction $\mathrm{SB} \propto (1+z)^{-4}$. A substantial deviation from the Tolman scaling was also found in other photometrically selected samples of spheroidal and elliptical galaxies (Pahre et al. 1996; La Barbera et al. 2003; Sandage 2010), and ascribed to luminosity evolution empirically determined from the fits.

6 Conclusion

A phenomenological approach to galactic angular diameters and surface brightness has been developed, by employing empirical fits rather than cosmic evolution equations derived from 'first' principles. The ingredients are scaling relations for the gravitational constant and the luminosity, based on the constancy of certain moderate ratios as in Dirac's theory (Dirac 1937; Dyson 1972), all in a Roberson–Walker

framework. The scaling exponents, mostly integer, are then inferred from the constant ratios and empirical fits. This may be regarded as a poor man's scaling approach to cosmology, detached from dark matter and cosmological constant. Neither the Einstein equations nor their various generalizations that go with varying constants are invoked. Such generalizations, e.g. Brans–Dicke and Kaluza–Klein theories, cf. Varshalovich et al. (2003), Setare and Jamil (2010) and references therein, are always ad hoc and have been tried for long with limited success. Therefore, it seems to be more promising to determine the cosmic expansion factor and other scale factors of varying fundamental constants empirically.

The idea behind varying constants is Dirac's large numbers hypothesis that moderate dimensionless ratios such as (1.2) and (5.1) or the electric fine-structure constant, $\alpha_e := e^2/(4\pi\hbar c) \approx 1/137$, stay constant throughout the cosmic evolution, otherwise it is difficult to explain why they are moderate just at the present epoch. The tightest bound on the present-day variation of α_e is $(-1.6 \pm 2.3) \times 10^{-8}$ Gyr^{-1}, obtained by testing the temporal change in the frequency ratios of atomic clocks (Rosenband et al. 2008; Kolachevsky et al. 2009). This bound surpasses the recent lunar ranging bounds on $\dot{G}_0/G_0$ by four orders, and makes a time variation of any of the three constants constituting α_e unlikely. Large dimensionless ratios, such as the ratio of electrostatic and gravitational force of attraction between an electron and proton, $e^2/(4\pi G_0 m_e m_p) \approx 2.3 \times 10^{39}$, can vary in cosmic time. A safe laboratory bound on the variation of the proton-electron mass ratio is $(-3.8 \pm 5.6) \times 10^{-5}$ Gyr^{-1}, obtained from frequency ratios of molecular and atomic clocks as defined by rovibrational and hyperfine transitions, cf. Shelkovnikov et al. (2008). We have adopted a pragmatic view, and showed that a varying gravitational constant $G \propto H(\tau)$ as suggested by the moderate ratio $\hbar^2 H_0/(G_0 c m_\pi^3)$ is useful to fit angular diameters and surface brightness. The purpose of this article is to demonstrate the efficiency of a phenomenological approach to observational cosmology detached from general relativistic evolution equations for the universe.

The mentioned ratios illustrate the meaning of the terms 'moderate' and 'large.' The precise value of ratio (1.2), the geometric factor $1/(4\pi)$, is not really important in this context; if we replace the pion mass by the proton mass, $m_p/m_\pi \approx 6.723$, or change the adopted value of the Hubble constant, $H_0 \approx 68.02$ km s^{-1} Mpc^{-1}, this ratio remains moderate. The fact that $G_0 c m^3 = 4\pi\hbar^2 H_0$ if we choose the pion mass for m and the mentioned value for H_0, is a remarkable coincidence if one considers which quantities and numbers are involved, but the reasoning in this article or in Tomaschitz (2005, 2010) does not depend on this specific value of the Hubble constant; a variation of H_0 within five percent can readily be accommodated in the fits. By contrast, a deceleration parameter very close to but different from -1 is essential.

Figure 1 provides a test of the cosmic expansion factor stated in the paper, cf. (2.1) and (3.8). This expansion factor was derived by taking into account the very tight bound on the time variation of the gravitational constant obtained from lunar laser ranging experiments, which implies, via the proportionality $G \propto H(\tau)$, a substantial constraint on the deceleration parameter, $|q_0 + 1| < 3 \times 10^{-3}$, cf. after (1.2). In Fig. 1, the redshift evolution of the angular-diameter distance, which is entirely determined by the cosmic expansion factor, is tested by plotting against the distances of galaxy clusters obtained from interferometric radio imaging and X-ray surface brightness. In brief, we advocate a Hubble constant $h_0 \approx 0.6802$, based on the above numerical coincidence, and a specific expansion factor defined in (2.1) and (3.8), with a deceleration parameter $q_0 + 1 \approx -2.786 \times 10^{-3}$. A cosmological constant or a dark matter density do not arise in this context. These concepts were introduced to rescue the Einstein equations in cosmology. As we avoid postulating cosmic evolution equations, there is no need to invoke 'dark energy' or to create a missing mass problem.

To summarize in slightly more technical terms:

(1) The redshift scaling $\propto 1/h(z)$ of the galactic linear diameters (4.1) in Figs. 4 and 5 is based on the varying gravitational constant $G = G_0 h(z)$, derived from the moderate dimensionless ratio (1.2); the scaling variable $h(z)$ is the normalized Hubble parameter, cf. after (2.6). The scale factor $1/h(z)$ also shows in the angular size–redshift relation (4.5), in particular in the angular-diameter fits of the rotator samples in Figs. 2 and 3.

(2) The scale factor $h^{2+\lambda}(z)$ of the surface brightness (5.3) is derived from the constant ratios (1.2) and (5.1) determining the redshift scaling of the gravitational constant and the galactic luminosity. The luminosity evolution $L \propto h^\lambda(z)$ also enters in the apparent magnitude–redshift relation (5.2) through the rescaling of the luminosity distance by a factor $h^{-\lambda/2}(z)$. The Hubble diagrams of the galaxy samples in Figs. 6 and 7 and their surface brightness evolution in Figs. 8 and 9 are fitted with the luminosity scaling exponent $\lambda = 9$, from which we infer the redshift scaling $v_G \propto h^2(z)$ of the galactic velocities in the microwave background, see after (5.1). The large luminosity exponent is required by a pronounced rise in the surface brightness of high-z galaxies, cf. Figs. 8 and 9, as well as by a decline of the apparent magnitude following the maximum attained at $z \approx 0.8$, see Figs. 6 and 7. By contrast, the SN Ia Hubble diagram in Tomaschitz (2010) only requires a mild luminosity evolution ($\lambda = 1$) of nearly perfect standard candles, cf. Stritzinger et al. (2006).

(3) The curvature radius of the 3-space enters only very weakly in the angular-diameter distance in Fig. 1, the angular size–redshift relation of the galaxy samples in

Figs. 2 and 3, and their Hubble diagrams in Figs. 6 and 7. The fits are consistent with a curvature radius above 4×10^4 Mpc, roughly ten times the Hubble distance c/H_0, cf. after (3.8). The crossover into the intermediate redshift regime is illustrated by the low-z expansions depicted as dotted curves in Figs. 2–9 and based on the ascending z series (2.7) and (3.5) of the Hubble parameter and the luminosity distance. In Fig. 1, the low-z expansion is indistinguishable from the plotted exact angular-size distance for $z \leq 1$.

(4) The linear-size evolution of the rotator samples in Figs. 4 and 5 indicates that galactic measuring rods are not very rigid indeed. The contracting galactic diameters and the fact that a flat 3-space geometry suffices to describe at least the low and intermediate redshift evolution in Figs. 1–9 suggest to use Euclidean space for cosmological modeling. The cosmic expansion factor (2.1) can be scaled into the fundamental constants, keeping their dimensionless ratios constant (Tomaschitz 1998, 2000a), so that Doppler shifts are generated by contracting atomic measuring rods, due to varying interaction constants in the Lagrangians. The redshift scaling relations discussed here on the basis of an expanding Robertson–Walker cosmology do not change, but contracting measuring rods in Euclidean space are conceptually simpler than a time dependent 3-space geometry. This also means to give up general covariance and consider the Lagrangians in an absolute spacetime conception (Tomaschitz 2003, 2007).

If coupling constants depending on cosmic time are substituted into covariant Lagrangians, the covariance is lost. In Brans–Dicke modifications of general relativity theory, covariance is enforced by turning the coupling constants into fields, which requires arbitrarily chosen insertions in the action functional to define these fields. Lagrangian mechanics works best if one starts with free fields and adds nonlinear interactions with small coupling constants. To turn fundamental constants into fields may be a logical possibility but is a little stretched, neither efficient nor in the spirit of Lagrangian mechanics. The natural setting for varying constants is the absolute cosmic spacetime. Once relativistic covariance is abandoned, a cosmic time scaling of the fundamental constants does not require any other alteration of the Lagrangians.

(5) The expansion factor defined in (2.1) and (3.8) is derived from paleoclimatic estimates of planetary surface temperatures (Tomaschitz 2005). We have shown that this expansion factor and the constant moderate ratios (1.2) and (5.1) can account for the redshift evolution of the angular-size distance in Fig. 1, the angular and linear diameters in Figs. 2–5, as well as for the apparent magnitude of the rotators in Figs. 6 and 7 and their surface brightness evolution in Figs. 8 and 9.

Acknowledgements The author acknowledges the support of the Japan Society for the Promotion of Science. The hospitality and stimulating atmosphere of the Center for Nonlinear Dynamics, Bharathidasan University, Trichy, and the Institute of Mathematical Sciences, Chennai, are likewise gratefully acknowledged.

References

Barthel, P.D., Miley, G.K.: Evolution of radio structure in quasars—a new probe of protogalaxies? Nature **333**, 319 (1988)

Blundell, K.M., Rawlings, S., Willott, C.J.: The nature and evolution of classical double radio sources from complete samples. Astron. J. **117**, 677 (1999)

Bonamente, M., et al.: Determination of the cosmic distance scale from Sunyaev–Zel'dovich effect and Chandra X-ray measurements of high-redshift galaxy clusters. Astrophys. J. **647**, 25 (2006)

Buchalter, A., et al.: Constraining Ω_0 with the angular size–redshift relation of double-lobed quasars in the FIRST survey. Astrophys. J. **494**, 503 (1998)

Dabrowski, Y., Lasenby, A., Saunders, R.: Testing the angular-size versus redshift relation with compact radio sources. Mon. Not. R. Astron. Soc. **277**, 753 (1995)

De Filippis, E., et al.: Measuring the three-dimensional structure of galaxy clusters. I. Application to a sample of 25 clusters. Astrophys. J. **625**, 108 (2005)

Dirac, P.A.M.: The cosmological constants. Nature **139**, 323 (1937)

Dyson, F.J.: The fundamental constants and their time variation. In: Salam, A., Wigner, E.P. (eds.) Aspects of Quantum Theory. Cambridge University Press, Cambridge (1972)

Gallagher, J.S., et al.: Supernovae in early-type galaxies: directly connecting age and metallicity with Type Ia luminosity. Astrophys. J. **685**, 752 (2008)

Gough, D.O.: Solar interior structure and luminosity variations. Solar Phys. **74**, 21 (1981)

Guenther, D.B., Krauss, L.M., Demarque, P.: Testing the constancy of the gravitational constant using helioseismology. Astrophys. J. **498**, 871 (1998)

Gurvits, L.I., Kellermann, K.I., Frey, S.: The "angular size–redshift" relation for compact radio structures in quasars and radio galaxies. Astron. Astrophys. **342**, 378 (1999)

Holanda, R.F.L., Lima, J.A.S., Ribeiro, M.B.: Testing the distance-duality relation with galaxy clusters and Type Ia supernovae. Astrophys. J. **722**, L233 (2010)

Kapahi, V.K.: Redshift and luminosity dependence of the linear sizes of powerful radio galaxies. Astron. J. **97**, 1 (1989)

Kolachevsky, N., et al.: Testing the stability of the fine structure constant in the laboratory. Space Sci. Rev. **148**, 267 (2009)

Komatsu, E., et al.: Seven-year Wilkinson Microwave Anisotropy Probe observations: cosmological interpretation. Astrophys. J. Suppl. (2010). arXiv:1001.4538

La Barbera, F., et al.: On the invariant distribution of galaxies in the $r_e - \langle\mu\rangle_e$ plane out to $z = 0.64$. Astrophys. J. **595**, 127 (2003)

Lacy, M., et al.: Optical spectroscopy of two overlapping, flux-density-limited samples of radio sources in the North Ecliptic Cap, selected at 38 and 151 MHz. Mon. Not. R. Astron. Soc. **308**, 1096 (1999)

Lubin, L.M., Sandage, A.: The Tolman surface brightness test for the reality of the expansion. IV. A measurement of the Tolman signal and the luminosity evolution of early-type galaxies. Astron. J. **122**, 1048 (2001)

Marinoni, C., et al.: Geometrical tests of cosmological models. III. The cosmology-evolution diagram at $z = 1$. Astron. Astrophys. **478**, 71 (2008)

Mason, B.S., Myers, S.T., Readhead, A.C.S.: A measurement of H_0 from the Sunyaev–Zeldovich effect. Astrophys. J. **555**, L11 (2001)

Müller, J., Biskupek, L.: Variations of the gravitational constant from lunar laser ranging data. Class. Quantum Gravity **24**, 4533 (2007)

Nakamura, K., et al.: Review of particle physics. J. Phys. G **37**, 075021 (2010)

Neeser, M., et al.: The linear-size evolution of classical double radio sources. Astrophys. J. **451**, 76 (1995)

Nilsson, K., et al.: On the redshift–apparent size diagram of double radio sources. Astrophys. J. **413**, 453 (1993)

Oort, M.J.A., Katgert, P., Windhorst, R.A.: A direct determination of linear size evolution of elliptical radio galaxies. Nature **328**, 500 (1987)

Pahre, M.A., Djorgovski, S.G., de Carvalho, R.R.: A Tolman surface brightness test for universal expansion and the evolution of elliptical galaxies in distant clusters. Astrophys. J. **456**, L79 (1996)

Percival, W.J., et al.: Baryon acoustic oscillations in the Sloan Digital Sky Survey Data Release 7 galaxy sample. Mon. Not. R. Astron. Soc. **401**, 2148 (2010)

Reese, E.D., et al.: Determining the cosmic distance scale from interferometric measurements of the Sunyaev–Zeldovich effect. Astrophys. J. **581**, 53 (2002)

Reid, B.A., et al.: Cosmological constraints from the clustering of the Sloan Digital Sky Survey DR7 luminous red galaxies. Mon. Not. R. Astron. Soc. **404**, 60 (2010)

Rosenband, T., et al.: Frequency ratio of Al^+ and Hg^+ single-ion optical clocks; metrology at the 17th decimal place. Science **319**, 1808 (2008)

Sagan, C., Chyba, C.: The early faint Sun paradox: organic shielding of ultraviolet-labile greenhouse gases. Science **276**, 1217 (1997)

Saintonge, A., et al.: Geometrical tests of cosmological models. II. Calibration of rotational widths and disc scaling relations. Astron. Astrophys. **478**, 57 (2008)

Sandage, A.: The Tolman surface brightness test for the reality of the expansion. V. Provenance of the test and a new representation of the data for three remote HST galaxy clusters. Astron. J. **139**, 728 (2010)

Sandage, A., et al.: The Hubble constant: a summary of the Hubble Space Telescope program for the luminosity calibration of Type Ia supernovae by means of Cepheids. Astrophys. J. **653**, 843 (2006)

Sandage, A., Reindl, B., Tammann, G.A.: The linearity of the cosmic expansion field from 300 to 30.000 $\mathrm{km\,s^{-1}}$ and the bulk motion of the Local Supercluster with respect to the CMB. Astrophys. J. **714**, 1441 (2010)

Setare, M.R., Jamil, M.: Holographic dark energy with varying gravitational constant in Hořava–Lifshitz cosmology. J. Cosmol. Astropart. Phys. **02**, 010 (2010)

Shelkovnikov, A., et al.: Stability of the proton-to-electron mass ratio. Phys. Rev. Lett. **100**, 150801 (2008)

Singal, A.K.: Cosmic evolution of the physical sizes of extragalactic radio sources and their luminosity–size correlation. Mon. Not. R. Astron. Soc. **233**, 87 (1988)

Singal, A.K.: Cosmic evolution and luminosity dependence of the physical sizes of powerful radio galaxies and quasars. Mon. Not. R. Astron. Soc. **263**, 139 (1993)

Sneden, C., Cowan, J.J., Gallino, R.: Neutron-capture elements in the early Galaxy. Annu. Rev. Astron. Astrophys. **46**, 241 (2008)

Stritzinger, M., et al.: Constraints on the progenitor systems of Type Ia supernovae. Astron. Astrophys. **450**, 241 (2006)

Teller, E.: On the change of physical constants. Phys. Rev. **73**, 801 (1948)

Tomaschitz, R.: Ether, luminosity and galactic source counts. Astrophys. Space Sci. **259**, 255 (1998)

Tomaschitz, R.: Cosmic time variation of the gravitational constant. Astrophys. Space Sci. **271**, 181 (2000a)

Tomaschitz, R.: Faint young Sun, planetary paleoclimates and varying fundamental constants. Int. J. Theor. Phys. **44**, 195 (2005)

Tomaschitz, R.: Superluminal cascade spectra of TeV γ-ray sources. Ann. Phys. **322**, 677 (2007)

Tomaschitz, R.: Effect of a varying gravitational constant on the SN Ia Hubble diagram, AGN luminosity evolution, and X-ray source counts. Astrophys. Space Sci. **325**, 259 (2010)

Tomaschitz, R.: Tachyons, Lamb shifts and superluminal chaos. Eur. Phys. J. B **17**, 523 (2000b)

Tomaschitz, R.: Conformal tachyons. Int. J. Mod. Phys. A **15**, 3019 (2000c)

Tomaschitz, R.: Superluminal radiation by uniformly moving charges. Physica A **320**, 329 (2003)

Varshalovich, D.A., et al.: Current status of the problem of cosmological variability of fundamental physical constants. In: Karshenboim, S.G., Smirnov, V.B. (eds.) Precision Physics of Simple Atomic Systems. Lecture Notes in Physics, vol. 627. Springer, Berlin (2003)

Williams, J.G., Turyshev, S.G., Boggs, D.H.: Progress in lunar laser ranging tests of relativistic gravity. Phys. Rev. Lett. **93**, 261101 (2004)